47th SME North American Manufacturing Research Conference, Penn State Behrend Erie, Pennsylvania, 2019

Determination of process induced dimensional variations of ceramic parts, 3d printed by extrusion of a powder-binder feedstock

Matteo Strano*, Kedarnath Rane, Guillaume Herve, Anna Tosi

Department of Mechanical Engineering, Politecnico di Milano, Milano, Italy
Corresponding author. Tel.: +39 02 2399 8520 / +39 348 9253127, E-mail: matteo.strano@polimi.it

Abstract

This paper aims at presenting a methodology for compensation of dimensional variation during production of ceramic parts via extrusion based additive manufacturing process. A systematic geometric deviation is measured in as printed (green) and as sintered parts. In the present study, a specially developed CNC extrusion unit is used for 3d printing onto a 3 degrees of freedom parallel kinematics table. Two ceramic feedstocks, alumina and zirconia, are procured and their processing route is illustrated. The generated, corrected and modified G codes are directly fed to the controller of the table and extrusion unit. Validation of the performance is carried out by multiple samples and repeated measurements. Experimental results exhibit effective compensation and significant improvement in the dimensional accuracy. The calculation of geometric deviations and the proposed parametric determination through optimization allow the reduction in global dimensional variation, which decreases all sort of systematic errors concurrently. The proposed procedure is easily transferable to other rapid prototyping machines and allows scalability based on achieved surface quality, manufacturing time, mass and dimensional measurement.

Keywords: 3D printing; ceramics; dimensional veriation; compensation

1. Introduction

Additive manufacturing, i.e. layer-wise assembling of parts from CAD data, is gaining more and more importance for rapidly producing complex shaped ceramic objects required in many technical and medical fields. The general additive manufacturing of ceramics was reviewed in 2014 [1], showing that many alternative technologies are available. A promising process is the Vat Photopolimerization [2]. The selective laser sintering and melting (SLS/SLM) techniques for additive manufacturing of ceramics is a main process, which has been recently reviewed in the rapid prototyping journal [3]. A recently developed process called as Extrusion based Additive Manufacturing (EAM) process uses powder injection molding (PIM) feedstocks (mixtures made of a solid metal/ceramic powder and a viscous polymeric binder) to build ceramic objects, layer by layer [4][5]. Most of the available printers use Cartesian configuration for moving the extruder and the table [6], whereas recently developed delta machines use a more complex control system due to their trajectories generation [7].

Rapid speed and building capacity, higher production volume, less inertia of the extrusion assembly are the reported merits of delta machines for 3D printing [8]. The EAM process also adopts the subsequent steps of PIM, like debinding and sintering to obtain final functional parts [9] and it can also be integrated with intermediate milling operations [10].

Dimensional accuracy is considered as one of the important criteria for selecting the process and majorly referred to machine capabilities. Increase in the requirements about the precision of manufactured parts, additive manufacturing also demands constantly minimal dimensional variation from intended part geometries [11]. Many studies have aimed at explaining the suitability of rapid prototyping (in particular additive manufacturing) for dimensionally accurate production of complex shaped parts [12,13].

Thus, various systems have been developed to monitor and compensate the dimensional deviations/errors, possibly down to a range of few micrometers [14]. The main categories of errors in 3D printing, namely geometric, kinematic and

thermal, have been addressed by research and many methods have been developed to reduce or compensate them [15]. The applicability of compensation methods depends on their behavior and level of complexity. For a machine tool, the implementation of the compensation method is generally carried out in three phases [16]:

a) Identification of errors: Analysis of machine structure and process behaviour. The influence of machine compliance errors is especially important for serial robots and for parallel manipulators (delta robots), where the compromise between the stiffness of machine elements and their dynamic capabilities are crucial [12].

b) Modelling and forecasting: Elaboration and inclusion of component variation model into a complex machine tool and/or process model, numerical forecasting of deviation/error values in operational conditions.

c) Compensation: Setting up of a compensation system, implementation of compensation algorithms to the control system.

In the EAM process for ceramics, the identification of the errors and its sources is a cumbersome activity. The geometrical variation of final sintered parts obtained from EAM process is due to dimensional errors occurring while printing, debinding and sintering.

- Printing errors are due to table acceleration, flow variation during extrusion and positioning accuracy; they interact with part volume and complexity to add variability if the process parameters (extrusion velocity, nozzle diameter, printing strategy) are not set well.
- Variations in powder loading, debinding temperature and heating rate during thermal debinding are factors which may be considered for controlling the dimensional stability.
- Major dimensional changes (shrinkage) are taking place during sintering step. Sintering errors are sourced from temperature gradient and variable flow of inert gas in the furnace.

Within this work, dimensional measurements are investigated to serve the objective of identification of dimensional errors in parts produced by EAM process. The study is limited to the analysis of geometric dimensions of green and sintered parts by varying material and printing process parameters. This kind of study is presented for the first time in the scientific literature, with respect to the EAM of binder/ceramic feedstock.

2. Experimental Plan and Details

The overall additive manufacturing process can be described as a sequence of 3 main steps: a) 3d printing by extrusion of a green 3D shape, b) solvent and thermal debinding and c) sintering. For each step, there are many parameters and conditions which influence how a sintered and green/as-printed part dimensions deviate from the original CAD definition. Part shapes, printing strategies, infill percentages, part orientations, printing velocity, layer height, debinding and sintering thermal cycles and conditions are among the most significant parameters for deciding the physical and mechanical properties of 3D printed ceramic/binder or metal/binder parts [17,18].

In our tests, two commercially available feedstocks loaded with ceramic powder (~60 vol. %) are used as a raw material for producing green 3d printed parts: alumina Al_2O_3 (Inmafeed K1008) and zirconia ZrO_2 (Inmafeed K1009). The binders used for producing these feedstock are water soluble PEG and polypropylene.

2.1. Printing by extrusion a green 3D shape

The delta robot shown in Fig. 1 moves by free trajectories generated through axes with parallel kinematics, while the extruder remains stationary. The synchronized printing movements on the X, Y and Z orthogonal axes are managed by multiple universal joints, kinematic chain links and linear guides. The extruder nozzle extrudes at a constant programmed material flow rate and the work table moves on the X, Y and Z axes for controlled deposition in 3D space. Open source software Slic3r is used to generate G-code by converting the desired CAD object into a layer-by-layer instruction set defining the toolpath which the printer follows. Each printing strategy can generate different results (according to the printing parameters) from the same initial specifications.

The feedstock materials used to produce the green parts have distinct extrusion temperatures, (145°C for Al_2O_3 and 175°C for ZrO_2). The printing parameters which have been kept constant in the study are: 100 °C - bed temperature, 0.5 - layer thickness to nozzle diameter ratio, 100% - target infill density.
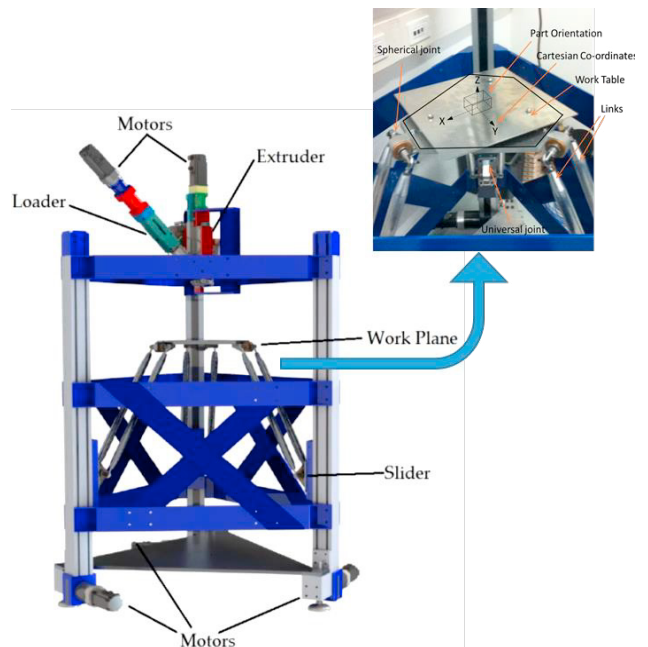

Fig. 1. Delta robot used in this study showing machine architecture for moving table and part coordinates. This table is part of the *Ephæstus* 3d printing machine developed at the Dipartimento di Meccanica of Politecnico di Milano.

2.2. Design of experiments

The parameters which have been changed in the design of experiments are:

- Feedstock material (which is confounded with the nozzle diameter); The machine adopted extruder nozzle with 0.4 mm diameter for alumina whereas for zirconia feedstock

nozzle with 0.8 mm diameter is used. This selection of 0.8 mm diameter nozzle is to improve the extrudability of zirconia feedstock.

- Printing strategy, which can be with or without the use of an outer perimeter made of 2 parallel roads.
- Part shape, which can be cylindrical, cubic or prismatic.
- Part orientation, which can be horizontal or vertical.
- Printing Velocity (mm/s), with levels given in Table 1.

The experimental plan is schematically presented with the aid of Fig. 2. Details of the geometrical and printing process parameters values used in the present study are given in Table 1. Two specimens (replicates) have been printed for each combination of material and process parameters.

The resulting plan of experiments is made of 120 combinations: 2 levels each for feedstock material, printing strategy and part orientation, 3 levels of part shape, 5 levels of printing velocity. Test parts are printed in a random sequence to limit the effect of extraneous parameters. The 240 parts are successfully printed using the Ephæstus machine shown in Fig. 1. Some representative green and sintered parts are shown in Fig. 2.

Table 1. Parameters used in the present study

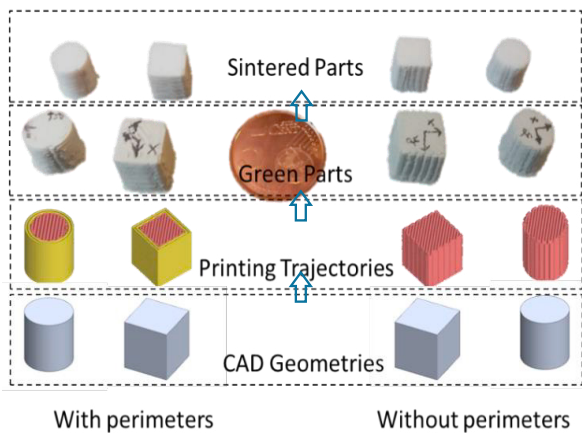| Control parameters	Levels
Feedstock material	Al_2O_3, ZrO_2
Printing strategy	2 perimeters, Zigzag (without perimeter)
Part shape	Cylinder, Cube, Rectangular bar
Part orientation	Horizontal, Vertical
Printing Velocity (mm/s)	7.5, 12.5, 17.5, 22.5, 27.5

Fig. 2. Schematic prospect of the experimental plan with 2 materials tested, 2 deposition strategies and measurement taken in the green and sintered states.

Simple shapes were modeled and supplied in STL format to get customized G-codes:

- cylinder with a diameter 10 mm and height 10 mm;
- cube with a constant cross sectional area of 10 by 10 mm;
- rectangular bar with 65 mm length, 10 mm width and 6 mm depth.

The nominal dimensions of the three tested shapes are aligned along the x-, y- and z-axis to facilitate the investigation of

external dimensions of parts in the green state and in the sintered state. After 3d-printing, a successive change of the geometrical dimensions is envisaged in order to evaluate the effect of the selected parameters as well as any interaction effects between these parameters.

2.3. Debinding and sintering

For the alumina feedstock, the debinding and sintering cycle is here described. Zirconia parts have not been sintered and are used to study only the printing characteristics.

A two-stage debinding method is used to remove the binder constituents from printed part. First step is solvent debinding, the parts are placed for about 24 hours in agitated water at 40 °C. Then parts are dried. Then thermal debinding is carried out in oven, by heating these parts at 300 ºC for 2 hours with a slow heating rate of 1 °C/min.

The alumina samples are finally sintered in tubular furnace with a heating rate of 5°C/min and then kept at 1600 °C for 1 hour.

2.4. Definition of dimensional deviations

The geometrical deviations can be measured after 3d printing (in the green state) and after sintering. They cannot be measured after debinding (in the so-called brown state) because the parts are too fragile to be handled.

To enable a uniform and reproducible determination of the occurring deviations, a measurement method is set up. The location of the measurement points are defined for each direction to allow a repeatability of the measurement. Three measurements are taken from different areas (top, middle and bottom) of each test part in this study. Dimensional data was obtained by direct measurement with an m-type Vernier digital caliper (model: Mitutoyo). From these measured values, a global (mean) dimension is evaluated for each part.

In the X printing direction, the main response variables investigated in this study are dXg, TXg, rX, drX, calculated using the following relations (1 – 6),

$$dXg_i = \frac{\text{X Dimension of green part} - \text{CAD nominal X dimension}}{\text{CAD X dimension}} \quad .... (1)$$

where i = 1, 2, 3 indicates the measurement location bottom, centre and top respectively

$$dXg = \sum_{i=0}^{3} dXg_i \quad .... (2)$$

$$TXg = \text{Max}(dXg_i) - \text{Min}(dXg_i) \quad .... (3)$$

$$rX_i = \frac{\text{X Dimension of green part} - \text{X Dimension of sintered part}}{\text{X Dimension of green part}} \quad ..... (4)$$

$$rX = \sum_{i=0}^{3} rX_i \quad .... (5)$$

$$drX = \text{Max}(rX_i) - \text{Min}(rX_i) \quad .... (6)$$

dXg and TXg indicate the dimensional precision of the printing process in the X direction; rX and drX isolate and indicate the dimensional precision of the debinding and sintering process. Similarly, the same variables have been measured in the Y direction. In the Z direction, only one deviation measurement dZg and one shrinkage measurement rZ has been taken, hence the vertical deviations TZg and drZ are not available.

3. Results

3.1. Dimensional deviation in green 3d printed alumina and zirconia parts

The Analysis of Variance (ANOVA) of the response variables is carried out to find out the significant factors. Figures 3 and 4 show the 95% confidence interval plots of the statistically significant parameters influencing the above stated responses, concerning dimensional variation in green parts. The plots demonstrate the trends in the mean percentage dimensional deviation as the function of printing velocity, feedstock material, printing strategy, part shape and part orientation.

The findings in the following sections report the dimensional variation in alumina and zirconia 3d printed parts. For these feedstocks, the best stability of the extruded filament, i.e. the best extrudability was obtained using a nozzle diameter $\varphi_n=0.4$ for the alumina and $\varphi_n=0.8$ mm for the zirconia. Clearly, a smaller nozzle diameter induces a better accuracy, therefore the better dimensional accuracy that will be presented for alumina parts is largely due to a smaller nozzle. Fig. 3 reports that the dimensional variation in X direction is lower than in Y direction, even by changing part orientation, feedstock material and nozzle diameter. This is because the part orientation in X directional is parallel to the one of the link (Fig. 1). Whereas the Y dimension of part is defined by combined movement of other two links of delta printer, which sources error in precise control of Y dimension.

A similar trend of higher dimensional deviation in Y direction is also reflected from Fig. 4. Fig. 3 also shows that the zirconia feedstock, which has proved to have a lower extrudability, is printed with larger errors as stated earlier. This interval plot also shows that by increasing printing velocity, the standard deviation in dX_g and dY_g significantly increases, although there is marginal increase in directional stability when only means are considered. Higher standard deviation with increasing printing velocity is a clear indication for lack of repeatability beyond 17.5 mm/s because increasing inertia forces limits the positioning accuracy of delta robot.

It is known that the outer perimeters in 3D printing play an important role to impart good surface finish. Surprisingly, Figure 4 demonstrates that the dimensional deviation in parts printed with perimeters is higher. The X-axis is more repeatable probably because it is aligned with one of the 3 machine links.

TX_g and TY_g (Fig. 5) effectively indicate the taper in Z direction. In fact, it is observed that cross section area of parts decreases with increasing build height (+Z direction). A reason could be a gravity effect that squeezes the bottom layers. The taper is also increased when higher nozzle diameter 0.8 mm is used in case of zirconia feedstock. Although the effects of material and nozzle diameter are confounded, it is reasonable to assume that a larger nozzle diameter, which provides a larger extruded flow rate, cools down more slowly. The part shape seems to have marginal effects on the taper, which confirms that the taper in green parts is mostly due to vertical thermal gradients and gravity.
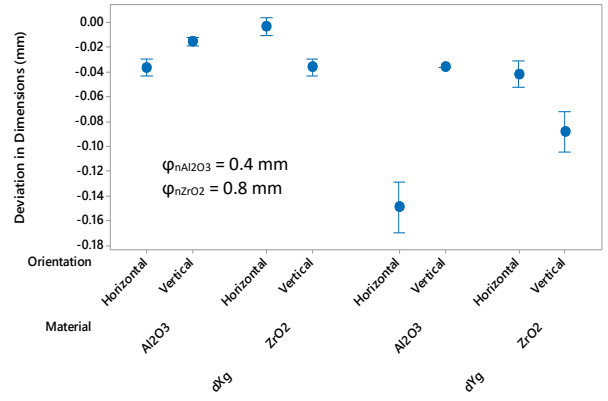

Fig. 3. Dimensional deviations (dXg on the left and dYg on the right) in green parts from their CAD geometries; the effect of part orientation is shown. The effect of the feedstock material is confounded with the nozzle diameter.
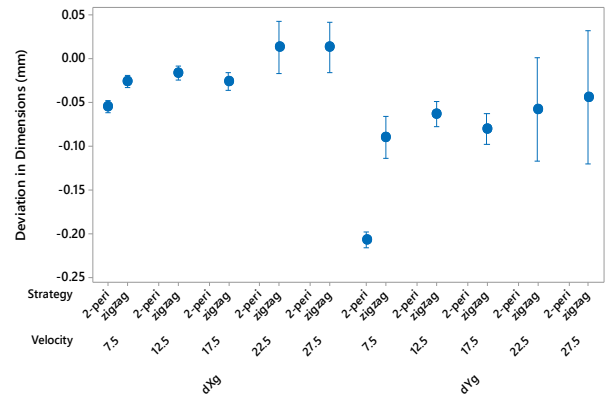

Fig. 4. Dimensional deviations (dXg on the left and dYg on the right) in green parts from their CAD geometries: effect of printing strategy (either with contour perimeter or only with a zig-zag infill and no contour) and printing velocity (mm/s)
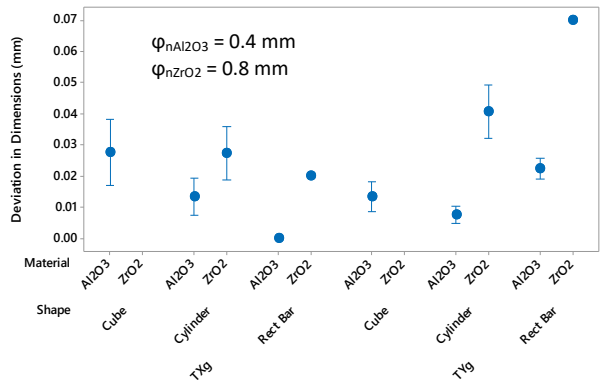

Fig. 5. Dimensional deviations (TXg on the left and TYg on the right) in the build direction for green parts: the effect of part shape (cube, cylinder or prismatic bar) can be observed. The effect of the feedstock material is confounded with the nozzle diameter.

3.2. Variable shrinkage in alumina sintered parts

A volumetric shrinkage after sintering was shown in Fig. 2. The mean values of the dimensional changes after sintering are determined for the alumina parts, and denoted as rX, rY and rZ using relations (4) and (5). The linear shrinkage is approximately estimated as 1/3 of the volumetric shrinkage if the effect of component geometry and material anisotropy is neglected. The volume % of binders for alumina feedstock is 40%, the approximate linear shrinkage should be 13.3%. However, the measured mean values of linear shrinkages are 11%, 12% and 14% in X, Y and Z direction respectively. While the measured linear shrinkage rZ value is constant and equal to 14%, the rX and rY values depend on the shape of the sample and in the table printing speed (Fig. 6).

Remarkably, the shrinkage decreases as the table speed increases. For the cubic and cylindrical samples, the shrinkage is isotropic in the X and Y direction. On the contrary, the rectangular bar, which has been printed with its longer side and the roads aligned with the X direction, has a significantly lower shrinkage in that direction. This is an indication that deposited material is denser in the direction parallel to the roads.
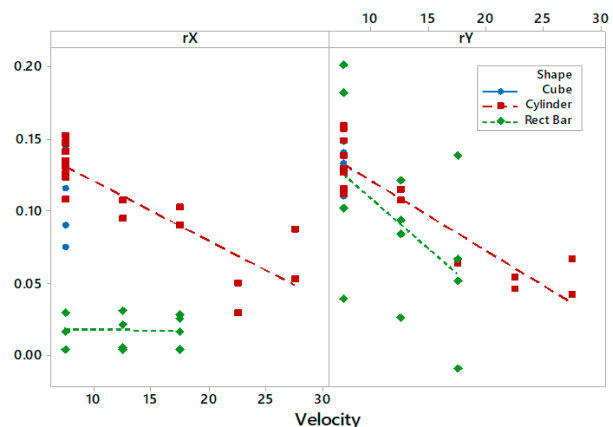

Fig. 6. Dimensional deviation rX (left) and rY (right) in sintered parts from their green part geometries: Effect of part shape and table speed (mm/s)
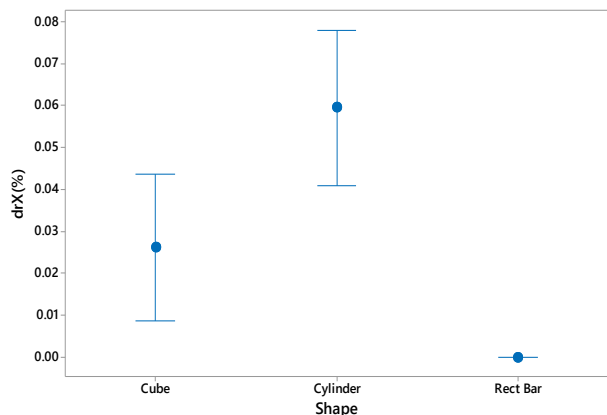

Fig. 7. Dimensional (drX) deviation in sintered parts from their green part geometries: Effect of part shape
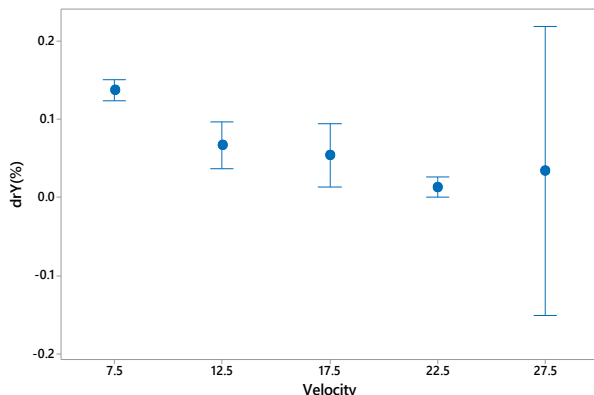

Fig. 8. Dimensional (drY) deviation in sintered parts from their green part geometries: Effect of printing velocity

Other important response variables are drX and drY, calculated using relation (6), that indicate the vertical uniformity of the shrinkage. Fig. 7 shows the effects of the part geometry on the shrinkage uniformity in the X direction, measured at different heights on the samples. Dimensional stability of rectangular bar shaped parts is higher because of their higher modulus (ratio of part volume to surface area).

Figure 8 shows the effects of the table speed on the uniformity of shrinkage in the Y direction, measured at different heights on the samples. It seems that printing at a speed between 17.5 and 22.5 mm/s reduces the shrinkage variation.

3.3. Discussion of results

Green and sintered parts have distinct dimensional variation from their nominal (CAD) dimensions, the progressive change in part volume after sintering is evident from Fig. 2. Parts with higher modulus (volume-to-surface ratio) show low volumetric shrinkage and the trend is similar as shown in Fig. 6 and 7 for any of the printing conditions. The effect of the table velocity on both the green deposition accuracy and the shrinkage is very significant. It is clear that at higher speed the machine can become less precise while printing, and this explains the role of speed on the green dimensional precision. Less trivial is the role of deposition speed on the shrinkage. Probably, extruding and printing at higher speed generates better compaction of the roads and the layers, and this reduces the shrinkage. After a compared analysis of Figures 4, 6 and 8, the printing velocity 17.5 mm/s can be taken as a good compromise between productivity, dimensional precision in the green state and shrinkage. The dimensional variations dXg, dYg, dZg, rX, rY and rZ can be easily compensated while printing, changing the g-codes accordingly, if their value can be predicted and if their variability is low. Their variability is given by the confidence intervals plotted in figures 3, 4, 5 and 6, which are smaller when printing in the X direction, with vertical orientation of samples, with table speed equal or lower than 17.5 mm/s.

Any difference in accuracy and variability between alumina and zirconia cannot be commented, because the effect of the material is confounded with the effect of the used nozzle diameters, which are different.

The compensation factor can be more easily determined when the TXg, TYg, drX and drY variables are small. This

generally happens when the table speed is equal or lower than 22.5 mm/s and it can be easily obtained with rectangular bars. The compensation factor is not a unique number because of the non-isotropic nature of geometrical variations and the interaction of process parameters. A simplified compensation model cannot be easily developed out of the present work, which represent a first step towards its development.

4. Conclusions

This paper investigates on the dimension variation and shrinkage behavior of ceramic parts 3D printed by extrusion of a binder/powder mixture. The results clearly show that the dimensional variations in as printed (green) parts and the shrinkage in sintered part are not uniform at the micro scale. They depend on the process parameters; they also depend on the material and part dimensions. Part with lower modulus exhibits higher relative shrinkage compared with a thicker section.

In general, the experimental investigations of materials and process parameters demonstrate that dimensional deviations could be reduced by an optimal selection of levels of different parameters. The table printing velocity should be controlled at 17.5 mm/s to improve on both the green deposition accuracy and the shrinkage, however this limits the productivity of process. Even though deposition speed, material and nozzle diameter are interacting parameters, they seem to have less significance on dimensional accuracy.

The paper has also shown that non-isotropic geometrical scaling factors which are derived by considering axis alignment and dimension from CAD. This scaling approach significantly minimizes the occurrence of deviations in the green parts and thereby limits variation in sintered part dimensions.

References

[1]   J. Deckers, J. Vleugels, J.P. Kruth, J. Ceram. Sci. Technol. 5 (2014) 245–260.
[2]   O. Santoliquido, P. Colombo, A. Ortona, J. Eur. Ceram. Soc. (2019) 0–1.
[3]   S.L. Sing, W.Y. Yeong, F.E. Wiria, B.Y. Tay, Z. Zhao, L. Zhao, Z. Tian, S. Yang, Rapid Prototyp. J. 23 (2017) 611–623.
[4]   T. Moritz, U. Partsch, S. Ziesche, U. Scheithauer, M. Ahlhelm, E. Schwarzer, H.-J. Richter, Additive Manufacturing of Ceramic Components, 2015.
[5]   S. Cano, J. Gonzalez-Gutierrez, J. Sapkota, M. Spoerk, F. Arbeiter, S. Schuschnigg, C. Holzer, C. Kukla, Addit. Manuf. 26 (2019) 117–128.
[6]   S. Iyer, J. Mcintosh, A. Bandyopadhyay, N. Langrana, A. Safari, S.C. Danforth, R.B. Clancy, C. Gasdaska, P.J. Whalen, Int. J. Appl. Ceram. Technol. 5 (2008) 127–137.
[7]   H. Giberti, L. Sbaglia, M. Urgo, J. Manuf. Syst. 43 (2017) 160–167.
[8]   B.M. Schmitt, C.F. Zirbes, C. Bonin, D. Lohmann, D.C. Lencina, A. da C.S. Netto, Mater. Res. 20 (2018) 883–886.
[9]   K. Rane, S. Cataldo, P. Parenti, L. Sbaglia, V. Mussi, M. Annoni, H. Giberti, M. Strano, in: AIP Conf. Proc., 2018.
[10] P. Parenti, S. Cataldo, M. Annoni, Manuf. Lett. 18 (2018) 6–11.
[11] D. Dimitrov, W. van Wijck, K. Schreve, N. de Beer, Rapid Prototyp. J. 12 (2006) 42–52.
[12] M.A.D. Shawn P. Moylan, John A. Slotwinski, April L. Cooke, Kevin K. Jurrens, in: Proc. Solid Free. Fabr. Symp., Austin (TX), 2012.
[13] C. Cajal, J. Santolaria, D. Samper, J. Velazquez, Rapid Prototyp. J. 22 (2016) 2–19.
[14] D.G.F. S. Fletcher, S.R. Postlethwaite, Trans. Eng. Sci. 23 (1999) 323–333.
[15] M. S., ed., Introduction to Precision Machine Design and Error Assessment, CRC Press Taylor & Francis Group, Boca Raton, 2009.
[16] L.C. H., Real-Time Error Compensation on Machine Tools through Optimal Thermal Error Modelling, University of Michigan, 1994.
[17] J. Gonzalez-Gutierrez, S. Cano, S. Schuschnigg, C. Kukla, C. Sapkota, C. Holzer, Materials (Basel). 11 (2018) 840.
[18] Clemens Lieberwirth, Arne Harder, Hermann Seitz, J. Mech. Eng. Autom. 7 (2017).